GEOPHYSICAL RESEARCH LETTERS, VOL. 24, NO. 18, PAGES 2343-2346, SEPTEMBER 15, 1997

# Volumetric imaging of aperture distributions in connected fracture networks

Laura J. Pyrak-Nolte

Department of Physics, Purdue University

Carlo D. Montemagno

Department of Agriculture and Bioengineering, Cornell University

David D. Nolte

Department of Physics, Purdue University

**Abstract.** We use x-ray computerized tomographic (CT) imaging to present quantitative aperture data for three-dimensional interconnected fracture networks imbedded in intact opaque rock samples several centimeters in length. X-ray images are obtained by injecting a high-density liquid metal into the fractured rock specimen under lithostatic conditions. The combination of tomographic reconstruction with gravimetric analysis makes it possible for the first time to obtain effective fracture aperture sizes to an accuracy of only several microns, located spatially within 300 microns. The apertures in the fracture network are spatially correlated over distances of 10 mm to 30 mm. The apertures of the intersections of the fractures were not found to be statistically larger in size than for the complete fracture network

## Introduction

The flow of natural and industrial fluids in rock formations cannot be understood without a detailed knowledge of the statistical and topographical geometry of fracture networks. Fractures are the dominant flow paths in rock, and fracture networks provide the conduits that control production rates at gas and oil wells in fractured reservoirs and control the migration rates of biologically hazardous materials, including nuclear, chemical and biological waste (Sahimi, 1993). Non-destructive imaging of three-dimensional fracture networks in natural rocks has been an elusive goal because rocks are opaque to most probes. Confocal microscopy can be used for near-surface imaging of pore geometry in rock (Montoto et al., 1995; Fredrich et al., 1995), as well as traditional photomicroscopy (Gretsch, 1995). However, confocal microscopy techniques for near-surface imaging of pores and cracks fail for depths greater than several hundred microns, necessitating destructive sectioning of the originally intact rock, and is time consuming for areas exceeding 1 $mm^2$. In addition, imaging of fracture geometry under simulated in-situ conditions, i.e. under equivalent lithostatic stresses at depth, has only recently become practical (Cook et al., 1993). In this report, we present the first three-dimensional aperture data of complex fracture networks within intact cores of opaque bituminous coal subjected to lithostatic conditions, and present the statistical and spatial distribution of fracture apertures within a single connected network, including all connected apertures down to two microns.



Paper number 97GL02057.
0094-8534/97/97GL-02057$05.00

## Samples

In our study, we have analyzed the three-dimensional geometry of fracture networks in four intact bituminous coal cores with 9 cm diameters and lengths ranging from 4 cm to 11 cm. Cores AA and BB were drilled from a single block of coal from Seam #1 in the Sundance Pit at the La Plata coal mine, San Juan Basin, San Juan County, New Mexico. The dimensions of the cores are given in Table 1. Core AA was drilled perpendicular to the bedding planes, while Core BB was drilled parallel to the bedding planes and parallel to the dominant fracture set (face cleat). Two additional coal cores IC2 and BC7A were whole drill cores from the Intermediate (IC) and the Basal (BC) Fruitland Formations extracted from depths of 545 m and 582 m, respectively, from the So. Ute #32-1 well, Valencia Canyon, San Juan Basin, La Plata County, Colorado, which is a gas-producing well. The Fruitland Formation (Upper Cretaceous) is estimated to contain 50 TCF of gas (Kelso et al., 1988) and is located in the world's most productive coalbed methane basin, i.e. the San Juan basin (Hill, 1993). Geometric fracture properties such as interconnectivity, porosity, orientation and aperture all play important roles in the recovery of methane at these sites.

## Experimental Procedure

The Wood's metal injection technique provides a unique tool for imaging fracture networks in opaque materials. In this technique, a low-melting-point metal is injected into samples under controlled stress conditions. The technique was originally developed for the investigation of pore geometry of sandstone (Dullien, 1969; Swanson, 1979), and subsequently has been applied to the investigation of the distribution of immiscible fluids within the pores of sandstone (Swanson, 1979; Yadav et al., 1984), crack growth under compressive stress (Zheng, 1989) and the contact area of single fractures (Pyrak-Nolte et al., 1987). In these previous studies, the metal casts of the pores were exposed by destructive sectioning or dissolution of the rock matrix for direct visual observation. We have extended the Wood's metal technique using X-ray imaging in conjunction with gravimetric measurements to image complex fracture networks within

intact core samples, obviating the need for destruction of the sample (Montemagno and Pyrak-Nolte, 1995) and improving the resolution of X-ray imaging of fracture apertures when no contrasting agent is used (Johns et al., 1993; Verhelst, et al., 1995). The Wood's metal provides a high-contrast material that facilitates x-ray tomographic analysis of the metal-filled fractures.

Prior to injection, a sample is placed in a hydrostatic pressure vessel and is subjected to the desired confining stress. The confining stress applied to each sample is given in Table 1. A nitrogen back pressure is applied to minimize oxidation of the coal cores during heating and to present a constant pressure front to the invading Wood's metal. In addition, the back pressure prevents the loss of moisture from the coal during heating, which is the principal cause of crack formation from the shrinkage of the coal matrix associated with moisture loss (Nelson, 1989). The injection system is heated to approximately 95 °C and the molten metal is injected into the coal core. After injection, the sample is cooled while the confining pressure and back pressure are maintained. When the metal has solidified, the sample is weighed to determine the weight of the injected metal. Using this gravimetric data and the density of the metal, the volume of injected voids is calculated. The smallest aperture penetrated by the metal is calculated using the surface tension of the metal, the pore pressure at solidification, and the capillary equation (Dake, 1978) for a cylindrical tube.

After the gravimetric analysis, the injected cores were scanned with a Philips Model Tomoscan 60/TX computerized x-ray tomographic (CT) system using 130 keV and a beam width of 2 mm. The spacing between x-ray scans (on the order of a millimeter) is given in Table 1 for all samples. Because of beam hardening artifacts (Kak and Slaney, 1988), standard morphological transformations (Jain, 1989) were applied to the data to correct for the exaggerated thickness of the metal-filled fractures in the x-ray scans (Montemagno and Pyrak-Nolte, 1995). The morphological transformations resulted in single-pixel localization of the metal-filled fracture. The pixel size in each scan for each sample is 0.3 mm x 0.3 mm. For volumetric analysis, the voxel (three-dimensional pixel) volume was 0.3 mm x 0.3 mm x $L_S$, where $L_S$ is the length between successive scans (given in Table 1).

## Results

There was a marked topological difference between the fracture networks in the various cores. Some cores exhibited sparse rectilinear features while others had less rectilinear and denser fracture sets. This imaging technique highlights morphological differences in different projections of the same fracture network.

A previous paper (Montemagno and Pyrak-Nolte, 1995) described the use of CT analysis to extract coal porosity. However, Pyrak-Nolte et al. (1993) have shown that porosity in coal cannot be directly related to permeability, which is the principal property of interest for flow analysis and prediction, because the aperture distribution (and specifically the spatial connectivity of the apertures) controls fluid movement through a fracture. Therefore, before it is possible to predict the flow properties of a network, it is necessary to extract quantitative values for the apertures and their spatial distribution.

We achieve this by relating the CT number of a specific voxel to the metal volume contained within that voxel (equation 1). This conversion relies on only two approximations: that the CT number is linearly related to metal volume in the voxel, and that the majority of voxels are spanned by only one fracture. The first approximation is based on the CT number being linearly related to density (Kak and Slaney, 1988) and that the density of a voxel will depend on the amount of metal in this voxel of the coal core. The second approximation must be checked for each coal sample. From field mapping of the western portion of the San Juan Basin high-volatile B bituminous coals (Laubach & Termain, 1991) and from inspection of all of the coal samples investigated here, coal cleats, the naturally occurring fracture networks, occur with well-defined fracture spacings of 6 mm to greater than 25 mm. Therefore, the only voxels that would contain more than one fracture are the intersections. In these voxels, the effective aperture size would be overpredicted. This overprediction will not affect one of our conclusions that fracture junctions do not have larger average apertures than the networks.

The aperture within the n-th voxel is obtained by multiplying the $CT_n$ number of that voxel by a factor F, which is constrained by the total volume of injected metal through the expression

$$F = d\frac{V_{grav}}{V_{vox}\sum_{n=1}^{N}(CT_n - CT_{coal})} \quad (1)$$

where the sum is over all voxels and $V_{vox}$ is the voxel volume, d is the linear size in the plane of a CT-slice (300 μm), $V_{grav}$ is the total volume filled by injected metal, and $CT_{coal}$ is the

Table 1. Data for Coal Samples IC2, BC7A, AA and BB.

| Sample Number | IC2 | BC7A | AA* | BB* |
|---|---|---|---|---|
| Length (mm) | 101.7 | 92.96 | 44.1 | 112 |
| Diameter (mm) | 91.6 | 91.6 | 88.9 | 88.9 |
| Bulk Volume ($cm^3$) | 670 | 624 | 274 | 694 |
| Confining Pressure at Solidification (MPa) | 7.22 | 8.19 | 4.89 | 5.54 |
| Nitrogen Pressure at Solidification (MPa) | 0.697 | 0.750 | 0.49 | 0.44 |
| Minimum Aperture Filled with Wood's Metal[1] (μm) | 1.78 ± 0.06 | 1.66 ± 0.06 | 2.44 ± 1.2 | 2.74 ± 1.3 |
| Weight of Injected Wood's Metal (grams) | 6.77 | 7.562 | 2.14 | 6.19 |
| Volume of Connected Voids($cm^3$) | 0.70 ± 0.019 | 0.759 ± 0.024 | 0.22 ± 0.005 | 0.65 ± 0.013 |
| Effective Cleat Porosity[2] (%) | 0.104 ± 0.0028 | 0.121± 0.004 | 0.082 ± 0.002 | 0.094 ± 0.002 |
| Spacing between X-ray Scans (mm) | 1.017 | 1.0 | 1.05 | 1.217 |
| Constant of Proportionality, F (x $10^{-5}$) | 5.25 | 3.28 | 7.11 | 5.03 |
| Minimum Aperture from Image Analysis (μm) | 2.25 | 1.77 | 2.22 | 2.62 |

[1]*Error from deviations in surface tension and contact angle of Wood's Metal* [2]*Error from deviations in the density of Wood's metal.*

* *From Montemagno and Pyrak-Nolte (1995)*

average CT density associated with the coal matrix. The constant of proportionality F is given for each sample in Table 1.

Figure 1 shows the aperture distribution for cores AA and IC2. The distributions for cores AA and BB, which are mutually orthogonal cores from the same fracture network, are both fit well by gaussian functions. For core AA, the gaussian function has a mean aperture size of 41 microns, while the mean aperture for core BB is 51 microns. Cores IC2 and BC7A, from a different coal formation, and originating 37 meters apart in the formation, are best fit by log-normal functions with most probable apertures of 22 microns and 24 microns, respectively. From the injection pressure data, the smallest aperture penetrated by the metal is in good agreement with the smallest aperture determined from the x-ray data (Table 1). The largest apertures observed in the cores ranged from 122 microns to 257 microns. Cores with few long fractures (e.g. IC2 in Figure 1) tended to have log-normal aperture distributions as compared with cores with many filamentary fractures (Core AA).

## Discussion

Using the unique set of aperture data obtained through this analysis, we can address several long-standing questions concerning the role of fractures in transport, the extent and role of spatial correlations, and the validity of extrapolating two-dimensional cross-sections into three-dimensional networks. For instance, the lines of intersection between two fractures within a network may hypothetically be preferentially composed of the largest apertures, which therefore may dominate fluid flow through a rock mass. Figure 2 shows the aperture distribution for the entire fracture network compared with the intersections alone for core BB. Both distributions of core BB are fit by gaussian functions with mean apertures that differ by only 12 microns. Similarly, the two distributions from core IC2 are fit by a lognormal function with no significant difference in the mean value. Therefore, we find no statistically significant difference in the aperture distributions of the intersections relative to the total network. This finding would discount fracture intersections as dominant flow paths in terms of larger apertures contributing to dominant flow. However, this conclusion cannot discount that the intersections may be preferentially connected across the core.

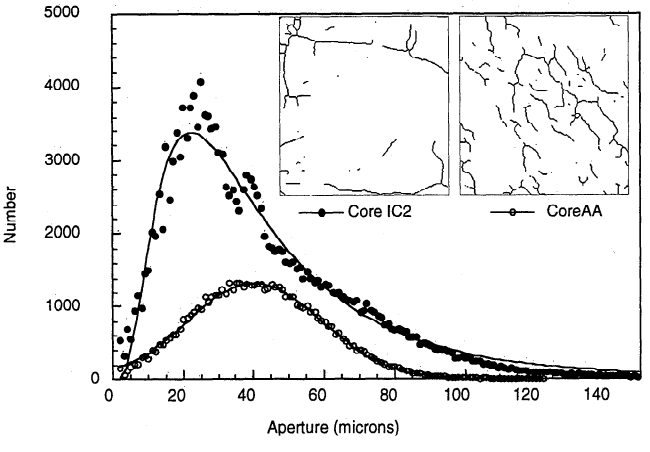


**Figure 1.** Aperture histograms for cores AA and IC2. Characteristic fracture network cross-sections are shown in the insets. The distributions for core AA is best fit by a gaussian function. Core IC2 is best fit by a log-normal function.

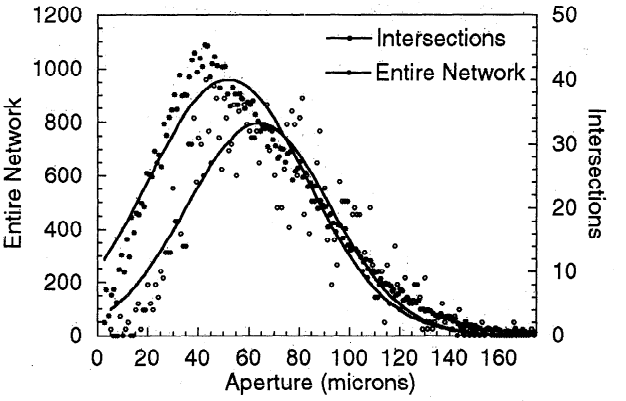


**Figure 2.** Aperture histograms for core BB comparing the distribution of apertures in fracture intersections to the total aperture distribution of the same core. Both distributions are fit by gaussians with means that differ by only 12 microns.

We examined the spatial correlation among the apertures within our volumetric dataset by performing a three-dimensional auto-correlation analysis on the three-dimensional fracture network. Figure 3 shows the autocorrelation functions for core AA and BB parallel to the axis of the core, and perpendicular to the axis of the core. The apertures in core AA and BB are correlated over distances of 6 mm to 30 mm and the correlation slope differs between the two-orthogonal directions (-0.92 vs -1.25). For core IC2, not shown in Figure 3, the apertures are correlated over distances up to 10 mm and exhibit approximately the same correlation slope (-0.87) for two orthogonal directions. In core BC7A, apertures are also scaling up to distances of 10 mm and the correlation slope is -1.2 and -0.9 for orthogonal directions. The difference in the correlation exponent for the two orthogonal directions suggests that the aperture network structure in cores AA, BB, and BC7A is a self-affine structure. These results show that three-dimensional extrapolations from two-dimensional cross-sections or rock outcroppings may not lead to faithful representations of fracture networks for distances that exceed the correlation length, which can be short. This point raises concerns about how well the three-

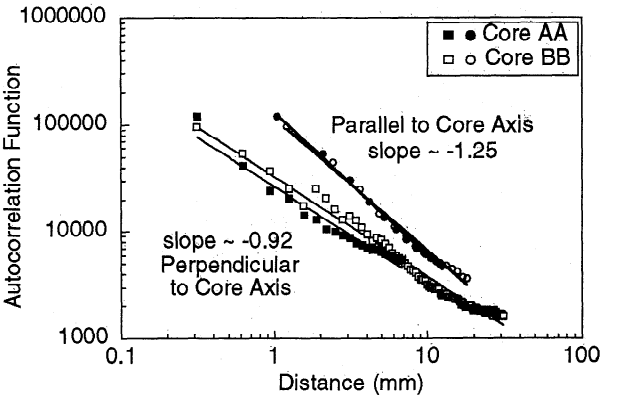


**Figure 3.** Autocorrelation functions for two-orthogonal directions for coal cores AA and BB based on a three-dimensional auto-correlation analysis.

dimensional fracture network presented here can be extrapolated to larger reservoir sizes. However, the fractures within these cores are the primary conduits that allow the transport of gas from the coal matrix into the larger scale fracture network.

## Conclusions

In conclusion, we have obtained quantitative values for the sizes and spatial distributions of fracture apertures inside single cores of opaque bituminous coal. The tomographic imaging of high-density and high-contrast metal injected into the fracture network under lithostatic conditions is combined with accurate gravimetric measurements to yield accurate values of the fracture apertures to within one micron uncertainty. This high accuracy is achieved despite a smaller accuracy for the spatial location of the fracture apertures within only 300 microns. The technique presented here is general and applicable for any fractured opaque rock or material. The unique and accurate data set provided by this technique should be valuable input for the understanding and modeling of fracture networks, and should provide direct answers for a broad range of related transport problems.

Acknowledgments. L. J. Pyrak-Nolte acknowledges support by the Gas Research Institute Contract Number 5092-260-2507, Amoco Production Research, and the NSF and ONR Young Investigator Awards. D. D. Nolte acknowledges support from the NSF Presidential Young Investigator Award.

## References

Cook, J. M., Goldsmith, G. and Auzerais, F., 1993, X-ray Tomography Studies of Wellbore Processes Under in situ Stress Conditions, Int. J. Rock Mech., vol. 30, No. 7, pp. 1091-1094.

Dake, L. P., Fundamentals of Reservoir Engineering, Elsevier Scientific Publishing Co., Oxford, 1978, pg. 347

Dullien, F.A.L., 1969, Determination of Pore Accessibilities - An Approach, Journal of Petro. Techno., vol 21, p14.

Dullien, F. A. L., 1981, Wood's metal porosimetry and its relation to mercury porosimetry, Powder Tech., v.29, p109-116.

Fredrich, J. T., Menendez, B., and T.-F. Wong, Imaging the Pore Structure of Geomaterials, Science, vol. 268, p2776,279, 1995.

Gertsch, L. S., Three-dimensional fracture network models from laboratory-scale rock samples, Int. J. Rock Mech. Min. Sci. & Geomech. Abstr., v. 32 (1), 85-91, 1995.

Hill, D. G., Coalbed Methane - State of the Industry, San Juan Basin, Colorado and New Mexico, Quarterly Review of Methane from Coal Seams Technology, v. 11 (1), 1993.

Jain, A. K., Fundamentals of Digital Image Processing, Prentice Hall, New Jersey, 1989.

Johns, R. A., Steude, J. S., Castanier, L. M., and P. V. Roberts, Nondestructive measurements of fracture aperture in crystalline rock cores using X-ray computed tomography, Journal of Geophysical Research, 98, 1889-1900, 1993.

Kak, A. C. and M. Slaney, Principles of Computerized Tomographic Imaging, IEEE Press, New York, 1988.

Kelso, B. S., Wicks, D. E., and V. A. Kuuskraa, A geologic assessment of natural gas from coal seams in the Fruitland Formation, San Juan basin, Gas Research Institute, Topical Report, GRI-88/0034, 56p, 1988.

Laubach, S. E. and C. M. Termain, Regional coal fracture patterns and coalbed methane development, Rock Mechanics as a Multidisplinary Science, ed. J.-C. Roegiers, Proceedings of the 32nd U.S. Symposium on Rock Mechanics, University of Oklahoma, 10-12 July 1991, A. A. Balkema, Rotterdam, 851-859.

Montoto, M., Martinez-Nistal, A., Rodriguez-Rey, A., Fernandez-Merayo, N., and P. Soriano, Microfractography of granitic rocks under confocal scanning laser microscopy, J. Microscopy, v. 177, pt. 2, 138-149, 1995.

Montemagno, C. D. and L. J. Pyrak-Nolte, 1995, Porosity of natural fracture networks, Geophys. Res. Lett., 22, 11, 1397-1400.

Nelson, C. R., 1989, Chemistry of Coal Weathering, Elsevier, New York.

Pyrak-Nolte, L. J., Myer, L.R., Cook, N.G.W., and P.A. Witherspoon, Hydraulic and Mechanical Properties of Natural Fractures in Low Permeability Rock, *Proceedings of the Sixth International Congress on Rock Mechanics*, eds. G. Herget & S. Vongpaisal, Montreal, Canada, August 1987, Pubs. A.A. Balkema (Rotterdam), pp.225-231, 1987.

Pyrak-Nolte, L.J., Haley, G. M., and B. W. Gash, 1993, Effective cleat porosity and cleat geometry from Wood's metal porosimetry, *Proceedings of the 1993 International Coalbed Methane Symposium*, Birmingham, Alabama, published by the University of Alabama, Tuscaloosa, Volume II, p639-647.

Sahimi, Flow phenomena in rocks: from continuum models to fractals, percolation, cellular automata, and simulated annealing, Rev. Mod. Phys., 65, 1393-1534, 1993.

Swanson, B.F., 1979, Visualizing pores and non-wetting phase in porous rock, J. Petroleum Tech., 31, pp.10-18.

Verhelst, F., Vervoort, F., De Bosscher, Ph., and G. Marchal, X-ray computerized tomography: Determination of heterogeneties in rock samples, Proceedings of the 8th International Congress on Rock Mechanics Tokyo, Japan, ed. T. Fujii, Publisher A. A. Balkema, Rotterdam, p105-108, 1995.

Yadav, G.D., Dullien, F.A.L., Chatzis, I. and I.F. MacDonald, 1984, Microscopic distribution of wetting and non-wetting phases in sandstones during immiscible displacements, SPE 13212, Society of Petroleum Engineers of AIME, Dallas, Texas.

Zheng, Z., 1989, Compressive Stress-Induced Microcracks in Rocks and Applications to Seismic Anisotropy and Borehole Stability, Ph.D. Thesis, University of California, Berkeley.

Prof. Laura J. Pyrak-Nolte, ,Department of Physics, Purdue University, West Lafayette, Indiana 47907 -1397

Prof. Carlo D. Montemagno, Department of Agriculture and Bioengineering, Cornell University, Ithaca, NY 14853

Prof. David D. Nolte, Department of Physics, Purdue University, West Lafayette, Indiana 47907 (e-mail: nolte@physics.purdue.edu)

(Received: August 16, 1996 ; Revised: March 21, 1997; Accepted April 17, 1997)